JACS
JOURNAL OF THE AMERICAN CHEMICAL SOCIETY
Communication
pubs.acs.org/JACS

Role of Electronic Perturbation in Stability and Activity of Pt-Based Alloy Nanocatalysts for Oxygen Reduction

Seung Jun Hwang,[†] Soo-Kil Kim,[†,‡] June-Gunn Lee,[§] Seung-Cheol Lee,[§] Jong Hyun Jang,[†] Pil Kim,[∥] Tae-Hoon Lim,[†] Yung-Eun Sung,[⊥] and Sung Jong Yoo*[,†]

[†]Fuel Cell Research Center and [§]Computational Science Center, Korea Institute of Science and Technology, 39-1 Hawolgok-dong, Seoul 136-791, Korea

[‡]School of Integrative Engineering, Chung-Ang University, 221, Heukseok-Dong, Dongjak-Gu, Seoul 156-756, Korea

[⊥]Center for Nanoparticle Research, Institute for Basic Science (IBS), and School of Chemical Biological Engineering, Seoul National University, Seoul 151-742, Korea

[∥]School of Chemical Engineering, Department of Hydrogen and Fuel Cell Engineering, Chonbuk National University, JeonJu, Jeonbuk, Korea

Supporting Information

ABSTRACT: The design of electrocatalysts for polymer electrolyte membrane fuel cells must satsify two equally important fundamental principles: optimization of electrocatalytic activity and long-term stability in acid media (pH <1) at high potential (0.8 V). We report here a solution-based approach to the preparation of Pt-based alloy with early transition metals and realistic parameters for the stability and activity of Pt_3M (M = Y, Zr, Ti, Ni, and Co) nanocatalysts for oxygen reduction reaction (ORR). The enhanced stability and activity of Pt-based alloy nanocatalysts in ORR and the relationship between electronic structure modification and stability were studied by experiment and DFT calculations. Stability correlates with the d-band fillings and the heat of alloy formation of Pt_3M alloys, which in turn depends on the degree of the electronic perturbation due to alloying. This concept provides realistic parameters for rational catalyst design in Pt-based alloy systems.

As interest in a hydrogen economy grows, research on hydrogen storage, hydrogen production, and fuel cells is expanding.[1] Polymer electrolyte membrane fuel cells (PEMFCs) are promising alternative devices for reducing our reliance on fossil fuels; however, several problems must be overcome to make them more economically attractive.[1] A pivotal issue is the large overpotential associated with the slow reaction rate of the oxygen reduction reaction (ORR) at the cathode.[2] This points to the need for better catalysts with decreased Pt content. Considerable efforts have been devoted to understanding the kinetics and mechanisms of the ORR in order to identify inexpensive and catalytically active electrocatalysts, such as bi- and multimetallic alloys.[2−5] Recent studies have looked for a correlation between electronic structure and the catalytic activity of metallic alloys for the ORR.[6] The adsorption energy of oxygen is proportional to the oxygen−metal bond strength and the position of the d-band center relative to the Fermi level. Another great challenge is the stability of electrochemical reactions, such as metal dissolution and surface oxide formation, which occur intensively in acid media (pH <1) at high potentials (>0.8 V).[4−7] Recently, the groups of Nørskov, Chorkendorff, and Yoo reported stable cathode catalysts of Pt alloyed with early transition metals, such as Hf, La, Sc, or Y.[7b−e] Markovic and Adzic et al. respectively demonstrated stable cathode catalysts of Pt alloyed with a 3d transition metal (especially, Pt-skin surface alloys) and of Pt modified with a Au cluster; in this manner, they emphasized the significance of stability considerations.[6a,8] Despite significant technological interest in finding active and stable catalysts for the ORR, direct experimental investigations into the contributions of the activities involving stability have rarely been performed on electrochemical reduction of oxygen.

We report realistic parameters elucidating stability and activity of Pt_3M (M = Y, Zr, Ti, Ni, and Co) alloy nanocatalysts prepared by high-pressure sputtering (see Supporting Information for experimental details). We focus on the electronic structure modification of the Pt_3M alloy nanocatalysts to identify the more active and stable electrocatalytic cathode materials. The results suggest that this concept has distinct merit, since significant changes in catalytic behavior and stability of Pt are observed for Pt-based alloy nanocatalysts made with early transition metals. Our results are an important step toward resolving serious problems and making PEMFCs economically viable.

To investigate and compare catalytic activities of ORRs with Pt_3M alloy nanocatalysts and pure Pt electrodes, we conducted hydrodynamic measurements in an O_2-saturated 0.1 M $HClO_4$ solution. Figure 1 shows the ORR polarization curves obtained for Pt_3M alloy nanocatalysts formed as thin-film rotating disk electrodes (RDEs). The catalysts activities, expressed as half-wave potential $E_{1/2}$, increased in the order Pt_3Ti < Pt < Pt_3Zr < Pt_3Co < Pt_3Ni < Pt_3Y. The Pt_3Y electrocatalyst had an extremely high activity, indicated by $E_{1/2}$ = 0.94 V, while its specific activity was 1.5 mA $cm^{-2}_{(real)}$ at 0.9 V; note that these values are similar to those of single-crystal $Pt_3Ni(111)$.[6a,d] To determine the various competing influences on this result, it is necessary to understand the ORR mechanism; however, there are numerous unresolved questions about the rate-determining step of the electrochemical

Received: August 9, 2012
Published: November 6, 2012

dx.doi.org/10.1021/ja307951y | J. Am. Chem. Soc. 2012, 134, 19508−19511

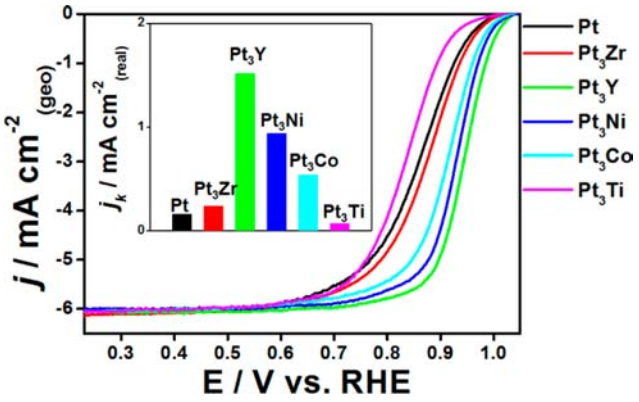

Figure 1. ORR polarization curves using Pt_3M (M = Y, Zr, Ti, Ni, and Co) alloy nanocatalysts and pure Pt nanocatalyst electrodes in 0.1 M $HClO_4$ solution; sweep rate, 10 mV s^{-1}; rotation rate, 1600 rpm. Inset: specific activity of Pt_3M electrodes expressed as kinetic current density (j_k) for ORR at 0.9 V.

reduction of oxygen.[9] The ORR mechanism is associated with a reaction wherein the oxygen adsorbed on the catalyst binds with an electron and a proton; along with the reactant oxygen and the final product water, several intermediates (O, OH, and OOH) are also involved.

When Pt_3Y alloys are used, changes in the electronic structure of Pt during the alloying facilitate the transition of the adsorbed OH to water by modifying the binding energy of the oxygen-containing species (OCS). Other parameters, such as the d-band center, can be helpful in discussing the Pt electronic structure. We measured the Pt_3M alloy d-band centers by synchrotron-based high-resolution X-ray photoelectron spectroscopy (XPS), as described previously.[10] The d-band center measurements enable us to directly correlate the catalytic activity variations during ORR with the variations in Pt_3M alloys. Pt d-band centers vs kinetic current density exhibit a volcano curve (Figure 2a), indicating that ORR activity is given by the OCS−Pt bond interaction strength, which depends on the Pt d-band states position relative to the Fermi level. However, if the position of the *d*-band centers of Pt becomes extremely high, the ORR currents decrease because they are blocked due to the OCS's stronger adsorptive bond strength. In the weak binding regime, barriers are high and limit the overall kinetics. In the strong binding regime, the kinetics are limited by the removal of products from the catalysts. These two regimes were seen in the so-called volcano plots where both weak and strong binding have low activity, and the active catalysts, providing a balance between these competing factors, are at the peak of the activity volcano. Using atomic oxygen binding as a reactivity descriptor for the ORR, a peak in activity is predicted at a binding strength slightly weaker than that on the surface of bulk Pt.

To reveal the nature of the stability of Pt_3M alloy catalysts used in electrocatalytic oxygen reduction, we compared with Pt_3M electrodes in an electrochemical environment (see Figure 2b). The Pt_3M stability effect was determined with an accelerated stability test, continuously applying linear potential sweeps from 0.6 to 1.1 V, causing cycles of surface oxidation/reduction of Pt. The accelerated stability measurements on a RDE were estimated by applying a potential sweep at 50 mV s^{-1} in an O_2-saturated 0.1 M $HClO_4$ solution at 25 °C. Metal dissolution and surface oxide formation occur in this potential region. Pt_3Y alloy nanocatalyst showed little decrease in activity after 3000 cycles (Figure 2b).

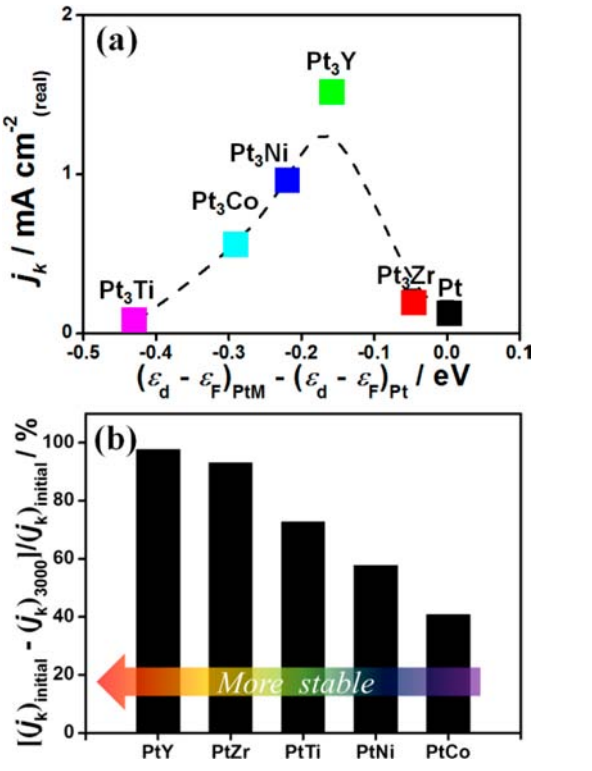

Figure 2. (a) Kinetic current density (j_k) at 0.9 V for ORR on Pt_3M (M = Y, Zr, Ti, Ni, and Co) alloy nanocatalysts and pure Pt nanocatalyst electrodes in 0.1 M $HClO_4$ solution, as a function of the measured d-band centers. The d-band centers were measured by high-resolution XPS (see Figure S6). (b) Histogram showing activity change of the polarization curves for ORR on Pt_3M alloy nanocatalysts on the RDE, before and after 3000 potential cycles (taken from Figure S5). Sweep rate, 10 mV s^{-1}; rotating rate, 1600 rpm.

Recently the ORR electrocatalytic stability was established as a function of either the thermodynamically calculated heat of alloy formation or the calculated oxygen binding energy.[11−16] Although those results provided valuable information, it was not possible to establish real systematic experimental trends. To date, electronic structure variations are employed to determine trends in the ORR electrocatalytic stability across the periodic table. At this point, it is important to emphasize that the relationships summarized in Figure 3 are unique in establishing a correlation between the theoretically determined intrinsic heat of alloy formation, stability, and the d-band vacancy on the Pt_3M. In

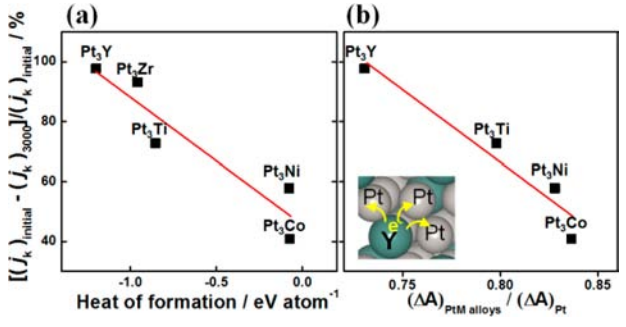

Figure 3. Correlation between stability (activity change of polarization curves before and after 3000 potential cycles) and (a) heat of alloy formation (from ref 19) and (b) absorption edge peaks of XANES spectra for Pt_3M (M = Y, Zr, Ti, Ni, and Co) catalysts.

dx.doi.org/10.1021/ja307951y | J. Am. Chem. Soc. 2012, 134, 19508−19511

particular, the relationship between stability and d-band vacancy on Pt_3M alloy catalysts is linear, implying that stability is susceptible to the d-band filling nature of the Pt_3M alloys.[12] To evaluate this, we measured X-ray absorption near-edge spectroscopy (XANES) on Pt_3M alloys as well as the Pt L_{III} edges. XANES analysis provides important information on the Pt d-band vacancy from an analysis of the Pt L_{III} white lines. Previously the fractional changes in the number of d-band vacancies relative to the reference material were estimated from differences between amplitudes for the Pt L_{III} absorption edges of the sample (pure Pt and Pt_3M alloys) and a Pt reference foil.[13] This technique represents a new method for examining the role of the alloying element in Pt alloys in the d-band vacancy of Pt. As shown in Figure 3b, the number of Pt 5d holes in the case of all the Pt_3Y alloy samples is the smallest among the Pt_3M alloy catalysts. The small vacancy in the Pt d-band is understood in terms of charge transfer from Y to Pt, lowering the d-band center of Pt (see Figures 2a and 5). Strong electronic interactions related to the heterometallic Pt_3Y bond formation with large (Pt) and small (Y) electronegativities might substantially influence the d-band vacancy shifts. Since the bulk electronegativity of Y (1.22) is considerably smaller than that of Pt (2.28), the formation of a metal−metal bond between Y and Pt induces the electron density to flow from Y to Pt. While the precise contributions of this effect to the experimentally observed lattice parameter shifts are still not fully understood, the two effects must be considered when analyzing d-band vacancy shifts.

Generally, dissolution of base metals, such as Co, Ni, or Fe, is believed to be responsibile for deactivation of Pt-based alloy systems.[14] Alloy system dissolution potentials affected by complicated parameters including surface segregation, atom size, water splitting efficiency, and hydroxyl ion adsorption energy.[16b] In terms of deactivation for Pt−early transition metal (ETM) alloy systems, Pt dissolution is more important than that of ETM because ETM in the Pt−ETM system has a more negative dissolution potential than Pt and is regarded a major deactivation factor. Indeed, different mechanisms may be required to elucidate deactivations of Pt−base metal and Pt−ETM systems. However, this trend in electron density flow from transition metals to Pt could provides realistic parameters for deactivation phenomena in Pt-based alloy system; more electron density flows from the second metal to Pt, giving greater stability under electrochemical reaction conditions.

Why do Pt−ETM alloys have exceptional stability and activity? We calculated the formation energy (E_0), cohesive energy (E_{coh}), and d-band center relative to Pt $[(\varepsilon - \varepsilon_F)_{PtY} - (\varepsilon - \varepsilon_F)_{Pt}]$ on tree-type Pt_3Y and Pt-slab, using DFT implemented in the Vienna ab initio simulation package code.[15] The exchange-correlation energy was evaluated within the generalized gradient approximation with the Perdew−Burke−Ernzerhof parametrization.[16] The electron relaxation was described by potentials with the projector augmented wave method.[17] Spin polarization and dipole correction were not considered in this study, except for individual atom cases, because several selected runs showed that they do not have a significant effect on calculation results. Geometries were considered to be optimized when the force on each atom was <0.02 eV $Å^{-1}$.

Before calculating and discussing Pt−ETM stability and activity, it is important to analyze the Pt−ETM surface structure in the electrochemical environment, a subject that is addressed in engineering catalysts for practical applications. Pt_3Y nanocatalyst surface analysis relies on angle-resolved XPS data, taken after soaking the sample in an electrochemical cell (0.1 M $HClO_4$ electrolyte) for 4 h. Figure 4a shows clear evidence of a catalyst surface skin composed of Pt with increasing depth and an increase in Y concentration until both Y and Pt reach a constant intensity, representative of the bulk composition. Figure 4b also suggests that there is a 1.0−1.5 nm Pt overlayer with a negligible amount of Y on the surface of Pt_3Y, observed via high-angle annular dark field scanning transmission electron microscopy (HAADF-STEM). On the basis of this experimental evidence, we first examined the possibility that the Pt-skin on Pt_3Y alloy nanocatalysts may be responsible for improving ORR. As shown in Figure 5 (inset table), Pt-skin structure is energetically

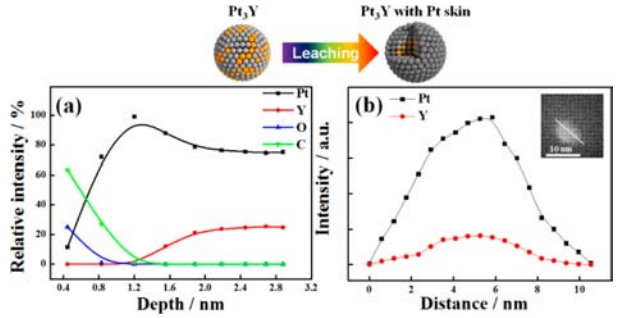

Figure 4. (a) Angle-resolved XPS profiles of Pt_3Y nanoparticles. (b) HAADF-STEM image and line profiles of Pt_3Y nanoparticles. Component distribution in line profiles clearly verifies the Pt-skin structure formation.

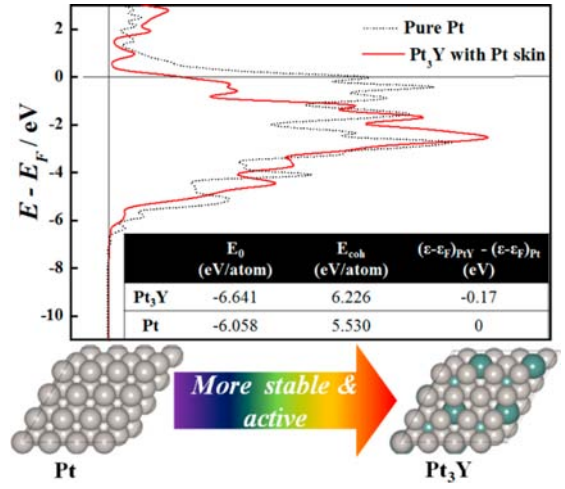

Figure 5. Pt and Pt_3Y with Pt-skin local density of state. Inset: properties of E_0, E_{coh}, and the d-band center relative to Pt $[(\varepsilon - \varepsilon_F)_{PtY} - (\varepsilon - \varepsilon_F)_{Pt}]$ on Pt_3Y with Pt-skin and Pt nanocatalysts.

favorable via E_0. A Pt atom in Pt_3Y is segregated to the surface or subsurface; the Y atom seldom exists as an isolated monomer on the surface. This indicates that, although there is a strong thermodynamic driving force toward dissolution of Y from Pt_3Y ($Y \rightarrow Y^{3+} = -2.72$ V vs NHE), the Pt-skin formation energy sets a significantly higher barrier for solute metal diffusion in this compound than in pure Pt or alloys of Pt with late transition metals. Recently, Greeley and Nørskov showed that the standard dissolution potential was roughly correlated with metal surface segregation energy.[18a−c] Jinnouchi et al.demonstrated that metal atoms with lower cohesive energy are less stable in solution (i.e., easily dissolve).[18g] To understand the Pt_3Y catalysts' high stability, we also calculated the cohesive energy via DFT calculations. Figure 5 (inset table) shows that the Pt_3Y cohesive

dx.doi.org/10.1021/ja307951y | J. Am. Chem. Soc. 2012, 134, 19508−19511

energy (6.226 eV/atom) is substantially higher than that of Pt (5.530 eV/atom).[18] Furthermore, the heat of Pt_3Y alloy formation is −1.2 eV/atom, sufficient to make these alloys thermodynamically stable against oxidation or dissolution in acid media. The Pt_3Y alloy catalysts' high stability can also be understood in terms of metal−metal d-bands that are approximately half-filled, implying that each of the two band elements contributes half of the nine d electrons for Pt, and Y contributes one d electron; moreover, the bonding states are filled, while the antibonding states are empty. Results from the study of the electrocatalytic trends of the Pt_3M alloy catalysts' stability can help explain the stability patterns as well as provide fundamentals for realizing improvements in alloy cathode catalysts.

We demonstrated that the relationship between kinetic current density and d-band center Pt_3M alloys exhibits a volcano curve trend, and we examined the Pt_3Y alloy structure and stability toward the ORR using first-principles quantum mechanical calculations. Our first-principles study shows that the ORR can be considerably affected by a surface Y atom surrounded by Pt atoms and the alloy formation of Pt_3Y with Pt-skin is energetically favorable. Further, the ORR stability is given by the d-band vacancy of Pt on the Pt_3M alloy electrodes as a function of electronic perturbation. Our current research suggests possibilities for stabilizing Pt-based alloy catalysts while simultaneously increasing ORR activity in electrochemical environments.

■ ASSOCIATED CONTENT

Ⓢ Supporting Information

Experimental details and characterization data. This material is available free of charge via the Internet at http://pubs.acs.org.

■ AUTHOR INFORMATION

Corresponding Author

ysj@kist.re.kr

Notes

The authors declare no competing financial interest.

■ ACKNOWLEDGMENTS

Work was supported by the Global Frontier R&D Program on Center for Multiscale Energy System funded by NRF under MEST, Korea. We are grateful to PLS for allowing us to conduct our XAS measurements. Y.E.S. acknowledges financial support by MEST through IBS program, Korea. Work was also supported by Future-based Technology Development Program through NRF funded by MEST (2009-0082471) and by the Joint Research Project funded by KRCF (Seed-10-2).

■ REFERENCES

(1) (a) Wang, C. Y. *Chem. Rev.* **2004**, *104*, 4727. (b) Besenbacher, F.; Chorkendorff, I.; Clausen, B. S.; Hammer, B.; Molenbroek, A. M.; Nørskov, J. K.; Stensgaard, I. *Science* **1998**, *279*, 1913. (c) Markovic, N. M.; Ross, P. N. *Surf. Sci. Rep.* **2002**, *45*, 117. (d) Nørskov, J. K.; Christensen, C. H. *Science* **2006**, *312*, 1322. (e) Wang, C.; van der Vliet, D.; More, K. L.; Zaluzec, N. J.; Peng, S.; Sun, S.; Daimon, H.; Wang, G.; Greeley, J.; Pearson, J.; Paulikas, A. P.; Karapetrov, G.; Strmcnik, D.; Markovic, N. M.; Stamenkovic, V. R. *Nano Lett.* **2011**, *11*, 919. (f) Ghosh, T.; Vukmirovic, M. B.; DiSalvo, F. J.; Adzic, R. R. *J. Am. Chem. Soc.* **2010**, *132*, 906. (g) Yoo, S. J.; Park, H.-Y.; Jeon, T.-Y.; Park, I.-S.; Cho, Y.-H.; Sung, Y.-E. *Angew. Chem., Int. Ed.* **2008**, *47*, 9307.

(2) (a) Appleby, A. J. *Catal. Rev.* **1970**, *4*, 221. (b) Adzic, R. R. In *Electrocatalysis*; Lipkowski, J., Ross, P. N., Eds.; Wiley-VCH: New York, 1998. (c) Srivastava, R.; Mani, P.; Hahn, N.; Strasser, P. *Angew. Chem., Int. Ed.* **2007**, *46*, 8988. (d) Savadogo, O.; Lee, K.; Oishi, K.; Mitsushima, S.; Kamiya, N.; Ota, K. I. *Electrochem. Commun.* **2004**, *6*, 105. (e) Mazumder, V.; Chi, M.; More, K. L.; Sun, S. *J. Am. Chem. Soc.* **2010**, *132*, 7848.

(3) Kinoshita, K., *Electrochemical Oxygen Technology*; Wiley: New York, 1992.

(4) Gasteiger, H. A.; Kocha, S.; Sompalli, B.; Wagner, F. T. *Appl. Catal., B* **2005**, *56*, 9.

(5) (a) Mukerjee, S.; Srinivasan, S. *J. Electroanal. Chem.* **1993**, *357*, 201. (b) Toda, T.; Igarashi, H.; Uchida, H.; Watanabe, M. *J. Electrochem. Soc.* **1999**, *146*, 3750. (c) Stamenkovic, V.; Schmidt, T. J.; Markovic, N. M.; Ross, P. N. *J. Phys. Chem. B* **2002**, *106*, 11970. (d) Zhang, J.; Vukmirovic, M. B.; Xu, Y.; Mavrikakis, M.; Adzic, R. R. *Angew. Chem.* **2005**, *117*, 2170. (e) Stamenkovic, V. R.; Moon, B. S.; Mayrhofer, K. J. J.; Ross, P. N.; Markovic, N. M. *J. Am. Chem. Soc.* **2006**, *128*, 8813. (f) Bae, S. J.; Yoo, S. J.; Lim, Y.; Kim, S.; Lim, Y.; Nahm, K. S.; Hwang, S. J.; Lim., T.-H.; Kim, S.-K.; Kim, P. *J. Mater. Chem.* **2012**, *22*, 8820.

(6) (a) Stamenkovic, V. R.; Fowler, B.; Mun, B. S.; Wang, G.; Ross, P. N.; Lucas, C. A.; Markovic, N. M. *Science* **2007**, *315*, 493. (b) Nørskov, J. K.; Rossmeisl, J.; Logadottir, A.; Lindqvist, L. *J. Phys. Chem. B* **2004**, *108*, 17886. (c) Zhang, J.; Vukmirovic, M. B.; Sasaki, K.; Nilekar, A. U.; Mavrikakis, M.; Adzic, R. R. *J. Am. Chem. Soc.* **2005**, *127*, 12480. (d) Stamenkovic, V. R.; Mun, B. S.; Arenz, M.; Mayrhofer, K. J. J.; Lucas, C. A.; Wang, G.; Ross, P. N.; Markovic, N. M. *Nat. Mater.* **2007**, *6*, 241.

(7) (a) Calvo, S. R.; Balbuena, P. B. *Surf. Sci.* **2007**, *601*, 4786. (b) Greeley, J.; Stephens, I. E. L.; Bondarenko, A. S.; Johansson, T. P.; Hansen, H. A.; Jaramillo, T. F.; Rossmeisl, J.; Chorkendorff, I.; Nørskov, J. K. *Nat. Chem.* **2009**, *1*, 552. (c) Yoo, S. J.; Kim, S.-K.; Jeon, T.-Y.; Hwang, S. J.; Lee, J.-G.; Lee, S.-C.; Lee, K.-S.; Cho, Y.-H.; Sung, Y.-E.; Lim, T.-H. *Chem. Commun.* **2011**, *47*, 11414. (d) Stephens, I. E. L.; Bondarenko, A. S.; Grønbjerg, U.; Rossmeisl, J.; Chorkendorff, I. *Energy Environ. Sci.* **2012**, *5*, 6744. (e) Stephens, I. E. L.; Bondarenko, A. S.; Bech, L.; Chorkendorff, I. *ChemCatChem* **2012**, *4*, 341.

(8) Zhang, J.; Sasaki, K.; Sutter, E.; Adzic, R. R. *Science* **2007**, *315*, 220.

(9) (a) Clouser, S. J.; Huang, J. C.; Yeager, E. *J. Appl. Electrochem.* **1993**, *23*, 597. (b) Sidik, R. A.; Anderson, A. B. *J. Electroanal. Chem.* **2002**, *528*, 69. (c) Greeley, J.; Rossmeisl, J.; Hellman, A.; Nørskov, J. K. *Z. Phys. Chem.* **2007**, *221*, 1209.

(10) Mun, B. S.; Lee, C.; Stamenkovic, V.; Markovic, N. M.; Ross, P. N. *Phys. Rev. B* **2005**, *71*, 115420.

(11) Denton, A. R.; Ashcroft, N. W. *Phys. Rev. A* **1991**, *43*, 3161.

(12) Mavrikakis, M.; Hammer, B.; Nørskov, J. K. *Phys. Rev. Lett.* **1998**, *81*, 2819.

(13) (a) Falicov, L. M.; Hanke, W.; Maple, M. P. *Valence Fluctuation in Solids*; North-Holland Pub.: Amsterdam, 1981. (b) Russell, A. E.; Maniguet, S.; Mathew, R. J.; Yao, J.; Roberts, M. A.; Thompsett, D. *J. Power Sources* **2001**, *96*, 226. (c) Mansour, A. N.; Cook, J. W.; Sayers, D. E. *J. Phys. Chem.* **1984**, *88*, 2330.

(14) (a) Chen, S.; Gasteiger, H. A.; Hayakawa, K.; Tada, T.; Shao-Horn, Y. *J. Electrochem. Soc.* **2010**, *157*, A82. (b) Hoshi, Y.; Yoshida, T.; Nishikata, A.; Tsuru, T. *Electrochim. Acta* **2011**, *56*, 5302.

(15) Kresse, G.; Joubert, D. *Phys. Rev. B* **1999**, *59*, 1758.

(16) (a) Perdew, J. P.; Burke, K.; Ernzerhof, M. *Phys. Rev. Lett.* **1996**, *77*, 3865. (b) Hammer, B.; Hansen, L. B.; Nørskov, J. K. *Phys. Rev. B* **1999**, *59*, 7413.

(17) (a) Kresse, G.; Furthmüller, J. *Comput. Mater. Sci.* **1996**, *6*, 15. (b) Blöchl, P. E. *Phys. Rev. B* **1994**, *50*, 17953.

(18) (a) Greeley, J.; Nørskov, J. K. *J. Phys. Chem. C* **2009**, *113*, 4932. (b) Jóhannesson, G. H.; Bligaard, T.; Ruban, A. V.; Skriver, H. L.; Jacobsen, K. W.; Nørskov, J. K. *Phys. Rev. Lett.* **2002**, *88*, 255506. (c) Greeley, J.; Nørskov, J. K. *Electrochim. Acta* **2007**, *52*, 5829. (d) Ma, Y.; Balbuena, P. B. *J. Phys. Chem. C* **2008**, *112*, 14520. (e) Shao, Y.; Yin, G.; Gao, Y. *J. Power Sources* **2007**, *171*, 558. (f) Menning, C. A.; Hwu, H. H.; Chen, J. G. *J. Phys. Chem. B* **2006**, *110*, 15471. (g) Jinnouchi, R.; Toyoda, E.; Hatanaka, T.; Morimoto, Y. *J. Phys. Chem. C* **2010**, *114*, 17557.

(19) http://databases.fysik.dtu.dk/.